BNL-108261-2015-JA

Frequency-comb referenced spectroscopy of ν_4- and ν_5-excited hot bands in the 1.5 μm spectrum of C_2H_2

Sylvestre Twagirayezu[a], Matthew J. Cich[b], Trevor J. Sears[a,b,], Christopher P. McRaven[a†], and Gregory E. Hall[a]*

[a] Department of Chemistry, Brookhaven National Laboratory, Upton, NY 1197; [b] Department of Chemistry, Stony Brook University, Stony Brook, NY 11794.

*Author to whom correspondence should be addressed. Electronic mail: sears@bnl.gov

[†] *Present address: Menlo Systems Inc., 56 Sparta Avenue, Newton, NJ 07860*

Abstract

Doppler-free transition frequencies for v_4- and v_5-excited hot bands have been measured in the $\nu_1 + \nu_3$ band region of the spectrum of acetylene using saturation dip spectroscopy with an extended cavity diode laser referenced to a frequency comb. The frequency accuracy of the measured transitions, as judged from line shape model fits and comparison to known frequencies in the $\nu_1 + \nu_3$ band itself, is between 3 and 22 kHz. This is some three orders of magnitude improvement on the accuracy and precision of previous line position estimates that were derived from the analysis of high-resolution Fourier transform infrared absorption spectra. Comparison to transition frequencies computed from constants derived from published Fourier transform infrared spectra shows that some upper rotational energy levels suffer specific perturbations causing energy level shifts of up to several hundred MHz. These perturbations are due to energy levels of the same rotational quantum number derived from nearby vibrational levels that become degenerate at specific energies. Future identification of the perturbing levels will provide accurate relative energies of excited vibrational levels of acetylene in the 7100-7600 cm^{-1} energy region.

Keywords: Acetylene, vibrational spectroscopy, energy levels, frequency comb, perturbations, sub-Doppler spectroscopy, Lamb dip

1. Introduction

Acetylene (ethyne, C_2H_2), has long been used as a model system for high-resolution infrared spectroscopic studies. Herman[1] , and Didriche and Herman[2] have recently reviewed spectroscopic work involving acetylene in its ground state, intramolecular dynamics and its use as a probe for chemical processes in astronomical bodies such as planets, cooler stars and star formation regions. Of particular relevance to the current measurements, high resolution Fourier transform infrared (FTIR) spectroscopic work by Kou *et al.*[3] and Keppler *et al.*[4] assigned transitions in the $\nu_1 + \nu_3$ combination band and multiple hot bands in the same region at wavelengths around 1.5μm. The spectra were revisited in 2002 by El Hachtouki and Vander Auwera[5] who also reported new measurements of the absolute line intensities. Robert et al. reported cavity-ring down spectroscopic data recorded in the same wavelength region[6] which added to the number of bands assigned, and these workers also created a database of published acetylene spectroscopic data up to 8600 cm^{-1} in vibrational energy. Herman et al.[7] had collected and collated data for vibrational levels in the major isotopic variants of acetylene to energies of more than 10 000cm^{-1} in 2003 and this work provides a comprehensive bibliography of published spectroscopic work to that date. The existing, longer wavelength, infrared data was collected and combined in a global fit in 2007 by Robert et al.[8]. Amyay *et al.* extended the work to include bands up to 8900 cm^{-1} and refined the analysis using a polyad-based systematic treatment of the perturbations that was reported in 2011[9]. Perry et al. recently [10] further extended the model by including published data up to vibrational energies of up to 13000 cm^{-1}. A comparable global analysis including data up to 9700 cm^{-1} has also been reported by Lyulin *et al.* [11, 12] Also recently, Yu. *et al.*[13] measured terahertz spectra of acetylene in the $\nu_5 - \nu_4$ difference band (0.8-1.6 THz, 26-53 cm^{-1}) with accuracy in line positions reported to be 100 kHz.

Vibration-rotation lines of acetylene in the 1.5 μm spectral region have been used as secondary frequency standards[14] and the main lines in this spectrum were some of the first measured using modern frequency comb-referenced instruments[15-17]. Aside from its intrinsic interest, the laboratory spectroscopic

work is crucial to applications in astronomy and remote sensing and acetylene has been detected in some star-forming regions of interstellar space[18] and in the atmosphere of Jupiter[19], Titan[20] and Earth[21, 22].

The development of very precise spectroscopic techniques based on phase-locked optical frequency combs[15, 16, 23] has opened up possibilities for routine, substantial, improvements in accuracy and precision compared to conventional laser techniques. Not only can absolute line positions be measured, but the frequency stability inherent in such instruments also permits concomitant improvements in line shape measurements. We have recently designed and built a spectrometer based on this technology and reported[24-26] measurements of temperature-dependent pressure broadening and shifts in the acetylene v_1+v_3 band. A major factor limiting the accuracy of the analysis of these data was found to be the presence of weak underlying lines[27] which, although having absorption strengths 100-1000 times smaller than the target absorption line, affect the line shape modeling because their absolute positions are imprecisely known. This issue has practical implications because remote sensing applications, such as those discussed above, rely on accurate laboratory measurements of line strengths and line shapes, and improvements in this area have a direct impact on the precision with which conditions and species concentration profiles may be extracted from remote measurements. In this work, we begin to address this problem by the measurement of accurate frequencies for hot band lines in the 1.5 μm acetylene spectrum derived from single excitation in the $\nu_4(\pi_g)$ (612.8 cm^{-1} excitation energy)[7] and $\nu_5(\pi_u)$ (730.3 cm^{-1} excitation energy)[7] fundamentals.

Here, we report 135 sub-Doppler line position measurements in the two hot bands (*i.e.* $(v_1v_2v_3v_4v_5)$ = (10110)-(00010) and (10101)-(00001)), and an analysis designed to identify perturbed upper state levels and make comparisons to previously published work involving the observed transitions. We estimate the root mean square error in the accuracy of the measured frequencies is typically less than 10 kHz. More details are given below.

2. Experimental

Sub-Doppler saturation dip spectroscopy has been used to determine rest frequencies for a series of absorption lines in the bands of interest. The experimental setup includes several modifications to that described previously [26]. Briefly, light from an extended cavity diode laser was locked to a mode of a resonant cavity-based absorption cell via the Pound-Drever-Hall technique [28]. The cavity was itself referenced to a frequency comb. The resulting spectrometer is capable of measuring molecular transitions with accuracy and precision approaching that of the frequency comb; that is to better than one part in 10^{11}. Changes from our original setup include a newly designed resonant cavity with a finesse of ~ 430, corresponding to mirror reflectivity of 0.9964 at this wavelength, a free spectral range of approximately 299.8 MHz, and the use of a home-made Er-doped fiber amplifier to increase the available probe laser power. Other changes include the design of the locking and feedback circuits to permit synchronous scanning of the cavity and comb stabilization. The new design offers increased sensitivity for weak transitions and better stabilization, thus improving the quality of the data.

A schematic diagram of the current apparatus is shown in Figure 1. The 50 cm-long cavity-type absorption cell used in the experiments was constructed of Invar, temperature-stabilized at 313.0K, and resided in a separate windowed vacuum chamber. The cavity mirrors were both held in mounts that could be adjusted by piezoelectric (PZT) actuators. One PZT with high bandwidth allowed a short travel while the second, slower one, was used for longer scans of the cavity length. The first of these was used for locking a selected cavity mode to a frequency comb component by the procedure outlined below, and for short scans of the cavity length during data acquisition. The second PZT could be used to scan modes through many hundreds of MHz to position a cavity mode to any desired frequency and permitted sawtooth-like sweeps of the cavity during setup and troubleshooting.

The output beam from an extended cavity diode laser (ECDL), operating near 1.5μm was split into two fractions. The first portion was frequency-modulated at 188 MHz using a resonant electro-optic modulator (EOM) (New Focus model 4003) driven by a voltage-controlled oscillator and combined with the comb output in a beat detection unit (Menlo Systems). The detector signal containing (among many others) the desired beat frequency between one of the two first order sidebands and a single comb component was processed through phase and frequency filters and amplifier (Menlo Systems BF020 and DXD200) to select the desired beat frequency signal. The processed beat frequency was then fed to a lock box (New Focus model LB1005) and the error correction signal relative to a chosen offset frequency (28.5 MHz, here) was applied to the higher bandwidth cavity PZT to lock a mode of the absorption cavity to a component of the frequency comb.

The second fraction of the ECDL light was directed into a home-made erbium-doped fiber amplifier (EDFA) resulting in up to 25 mW of output power, although not all of this was used for these experiments. The output from the EDFA was frequency-modulated at 192 MHz in a second resonant EOM and directed into the absorption cell. The 192 MHz phase modulation permitted Pound-Drever-Hall (PDH) locking of the laser to the cavity[28]. The amplified signal from the PDH detector was mixed down (Figure 1) and processed by a second LB1005 lockbox. The resulting error correction signal with a 300 kHz bandwidth was applied to the injection current of the ECDL via a high bandwidth (0-2 MHz) bias tee connection. These two locking loops effectively hold the ECDL, cavity and comb fixed relative to one another to a precision close to that of the frequency comb itself.

Tuning of the spectrometer was achieved by stepping the comb repetition rate by a fraction of a Hz at a time. The feedback loops described above keep the ECDL frequency, as well as the cavity, offset locked to a scanning frequency comb line.

In order to measure a derivative of the cavity transmission signal as the system was scanned, an audio frequency (~ 830 Hz) dither at an amplitude of approximately 0.2 MHz was also applied to the 188 MHz modulator used for the ECDL-comb locking loop. To detect the molecular absorption signal, the transmitted power through the cavity was detected using an InGaAs photoreceiver (New Focus) and processed in a digital lock-in amplifier at the audio frequency. The absorption cavity fast PZT and the ECDL cavity PZT also had separate samples of the same audio frequency signal applied to them with both phase and amplitude chosen to eliminate the empty cell signal detected at this frequency on the transmitted light in order to minimize locking error breakthrough at the audio frequency . Saturation dips then appear as first derivatives of a Lorentzian line shape transmission signal.

Pressures of between 3 and 32 mTorr (0.4-4.3 Pa), measured using a capacitance manometer with 1 Torr (133.3 Pa) full scale range, of purified[26] acetylene were used for the new measurements, depending on the strength of the absorption line under study. Comparison of multiple individual line frequencies in the $\nu_1 + \nu_3$ band measured in our laboratory with those previously reported in the literature[16], showed a root mean square deviation of 3 kHz between the measured and published frequencies, confirming the accuracy of the spectrometer. There is a slight statistical tendency for our measured frequencies to be higher, by several kHz, compared to those reported by Madej et al.[16] and this may be due to the lower pressures employed in the present work compared to the standard 20 mTorr employed by them. For the $\nu_1 + \nu_3$ P(11) line, the measured pressure shift coefficient is -0.00806 cm^{-1}/atm[25] corresponding to -0.32 kHz/mTorr. Hence, pressure shifts of up to ~10 kHz may limit the absolute accuracy of the hot band line frequencies at the highest pressures (32 mTorr) used for the measurements of weaker lines, assuming the pressure shift coefficient for P(11) is valid for the hot band lines. We attempted to measure a pressure shift in the sub-Doppler lines, but could not determine one due to the limited range of pressures that a single line could be observed with good signal-to-noise ratio, and also because of limited accuracy in the pressure measurements

due to the resolution of the manometer. The second issue will be eliminated in the future with a higher accuracy low-pressure gauge.

Typical line frequency measurements result from scanning the comb repetition rate by 0.25 Hz steps across the saturation dip, dwelling at each data point to collect an averaged transmission derivative signal. A single scan of ~ 20 MHz in the ECDL frequency required approximately 5-10 minutes to complete. At least 3 scans were made per line and the average line position is reported. No evidence for any contamination of the spectra caused by impurities in the cell was observed. The cell was pumped with a diffusion pump to less than 10^{-4} Torr and refreshed with a new sample several times a day. A remaining slow pressure rise of approximately 2 mTorr/hour was typically observed, probably due to residual outgassing of the vacuum chamber walls and cell material.

3. Results and Analysis

Sub-Doppler scans of P(11) of the $\nu_1 + \nu_3$ band at a series of increasing laser powers are shown in Figure 2. These spectra were recorded at a pressure of approximately 1 mTorr (0.133Pa). Examples of hot band line measurements are shown in the upper panel of Figure 3. The saturation dip line shape function is expected to be Lorentzian and in order to determine the center of the absorption, i.e. the zero crossing of the derivative shape obtained here, the measured profile was fitted to either a simple difference of Lorentzians, representing an approximation to the expected derivative lineshape, or the first harmonic Fourier component of the Lorentzian line shape function using the expressions derived by Axner et al.[29]. The resulting fitted function was used to estimate the required center position. Negligible differences were found in the estimates of the line center for a particular scan and its uncertainty when either model was used, but fits to the analytical expressions from Axner et al. permitted estimates of the Lorentzian and modulation widths from measured profiles. Examples of the fits are shown in Figs. 2 and 3.

At the highest powers shown in Fig. 2 (corresponding to up to 82 mW of laser power in the cavity as estimated from the transmitted power on a cavity mode and the cavity finesse) the saturation dip line width increases, presumably due to power broadening, and an unsymmetrical line profile can be easily observed for the lines in the cold band.[30, 31] The weaker hot band lines were less easily saturated and no asymmetries were observed in them. Observed Lorentzian line widths (FWHM) under low pressure and low power conditions were approximately 470 kHz as determined by fitting the measured profiles to the Axner et al.[29] model. Following the analysis below, we attribute this to transit-time broadening. Simple theory for transit-time broadening[32] gives:

$$\delta\omega_{TT} = 2\pi\delta\nu_{TT} = 2\frac{c^*}{w}\sqrt{2ln2}. \qquad (1)$$

Where $\delta\omega_{TT}$ is the full-width half-maximum transit-time width in angular units $\delta\nu_{TT}$ is the same quantity in cycles/sec (Hz), c^* the most probable absorber speed (447 ms^{-1} for acetylene at 313K, as appropriate here) and w the radius of the beam waist in the cavity. Evaluating this for a cavity beam waist radius of 0.50 mm

(obtained by assuming a parallel input laser beam of 1mm diameter, mirrors of 0.50 m focal length, laser wavelength of 1.55×10^{-6} m, and ideal Gaussian optics) results in an estimated transit time broadening, $\delta\nu_{TT}$, of 360 kHz. The estimated transit-time line width of 470 kHz would correspond to a beam waist radius of 0.36 mm, within the expected error of the geometrical optics estimate above.

In order to calculate the saturation power, we start with Equ. (35) of Šimečková et al.[33] in cgs units:

$$S_{HIT}(T) = I_a \frac{\nu_0}{Q_{tot}(T)} \frac{8\pi^3}{3hc} e^{-c_2 E''/T} \left(1 - e^{-\frac{c_2\nu_0}{T}}\right) g_1 \mathcal{R}_{12} \times 10^{-36} \qquad (2)$$

where $S_{HIT}(T)$ is the HITRAN linestrength in cm.molecule^{-1} units, $Q_{tot}(T)$ is the partition function,[34] both at temperature T, I_a is the isotopic weight (0.978 here), c_2 is (hc/k_B) and $\mathcal{R}_{12} = |R_{12}|^2/g_1$ is the weighted transition moment square that will be in (Debye)^2 units here. $g_1 = g_{nspin}\times g_J$ for the degeneracy of the lower level. Note that the HITRAN inclusion of the M_J degeneracy in this factor results in effective rotational Hönl-London factors that are $(2J+1)$ times smaller than the standard definition[35]. The other symbols have their usual meanings. $S_{HIT}(296)$ for P(11) of the $\nu_1+\nu_3$ band is 1.165×10^{-20} cm.molec^{-1}[36] and converting to the temperature of the current measurements (313K) using Eq. (2), lower state energies from HITRAN2012, and the results of [34] we find $S_{HIT}(313)$ is 1.112×10^{-20} cm.molec^{-1}. Substituting in all the quantities and converting to SI units, we find $|R_{12}|^2 = 6.22\times10^{-64}$ C^{2}m^2. From Mazzotti et al.[37], we can estimate the saturation intensity as

$$I_s = \frac{\varepsilon_0 c\hbar^2}{2}\frac{\Gamma_{TT}^2}{R_{12}^2} \qquad (3)$$

where Γ_{TT}^2 is the squared relaxation rate appropriate for the transit time broadening. Γ_{TT} is assumed to be $2\pi\times0.470$ MHz here, from above, and Eq. (3) gives $I_s = 207$ mW/mm^2. Assuming the beam waist radius in the cavity is 0.36 mm (above), the saturation power is 83 mW at the beam waist. From measurements of the transmitted power at the peak of a fringe, we estimate the maximum intra-cavity power used in the measurements reported here is 120-140 mW. The line shapes in Fig. 2, recorded at powers of up to 82 mW,

show broadening indicative of strong saturation at the higher powers, hence the degree of saturation is of order unity or higher for the cold band lines, consistent with the saturation power estimate above.

Following similar arguments for the corresponding P(11) lines for ortho- C_2H_2 in the v_4- and v_5-excited hot band lines, saturation intensities are 233 mW/mm^2 and 242 mW/mm^2 corresponding to saturation powers of 93 mW and 97 mW respectively at the beam waist. Power broadening was easily observed in hot band lines recorded with intracavity powers of greater than 100mW.

All measured line positions for v_4 and v_5 hot band lines in the $\nu_1 + \nu_3$ band of acetylene are listed in Tables I and II and examples of data are shown in Fig. 3. The quoted errors in the measurements (column 4 of the tables) are estimates based on a combination of the 3 kHz accuracy determined from measurements of the $\nu_1 + \nu_3$ band lines described in the previous section, with the RMS error ($rmse_i$) estimate derived from the fitting of the line center position for the measurement *(i)* as $\boldsymbol{Error(i)} = \sqrt{\boldsymbol{3^2 + (rmse_i)^2}}$. The high frequency gain curve of the EDFA and the ECDL power limited measurements in the *R*-branch regions of the spectra to rotational levels values below *J*=12 and *J*=15 in the v_5 and v_4 hot bands, respectively. The lower panel of Fig. 3 is a stick spectrum illustrating the extent of the measurements. This was generated from the measured frequencies and assuming relative intensities at 296 K from HITRAN [5, 36]. Intensities for Q-branch lines, not listed in these references, were estimated from the intensity for the corresponding *R*-branch line by ratioing the appropriate Hönl-London factors[35].

The present measurements were first compared to data in the HITRAN2012 [36] database. The HITRAN frequencies were synthesized from parameters obtained by fitting to the FTIR data of references [3, 4] and we found that the published Kou et al.[3] parameters reproduced the HITRAN data to well within the FTIR experimental error. El Hachtouki and Vander Auwera [5] quoted identical wavenumber frequencies, also derived from the Kou et al. parameters. Differences between our measurements and HITRAN2012 were

computed and are shown in the column 5 of tables I and II. The *J*-dependent differences between the present measured frequencies and HITRAN are generally within the estimated HITRAN error of 30 MHz except for transitions involving certain *J*-values in the ν_4 hot band and these are clearly seen in Figure 4. There is a systematic, predominantly negative, difference for the ν_5 hot band lines.

To identify perturbed upper levels more clearly, the upper term values were first calculated by adding the appropriate lower state term values obtained from the Kou et al.[3] parameters to the wavenumber of each measured transition for the hot bands. While the absolute ν_4=1 and ν_5=1 energies are subject to unknown inaccuracy due to the comparatively limited precision of the measurements from which the parameters were determined, these levels are isolated and not subject to *J*-dependent perturbations. The upper levels so derived were then fit to a similar polynomial form:

$$E(J) = G_v + Bx - Dx^2 + Hx^3 \pm \frac{1}{2}\left[q_B y + q_D y^2 + q_H y^3\right], \qquad (4)$$

where $x = \left[J(J+1) - k^2\right]$, $y = J(J+1)$ and $k = l_4 + l_5 = 1$ here. G_v, B, D, and H represent, respectively, the vibrational energy, effective rotational constant, and effective centrifugal distortion constants while the q are rotational *l*-type resonance constants. The upper and lower signs in Eq.(4) represent *f* and *e* levels, respectively.

The fitting proceeded by first eliminating upper energy levels involved in transitions for which comparison to the HITRAN2012 data showed differences greater than 30MHz. These levels, as shown in the Fig.4 and listed in Tables I & II, are clearly perturbed. Further, upper levels giving larger residuals were also identified as probably perturbed, and subsequently removed from the fit (Supplementary Tables, S1 & S2). The final upper level parameters determined from this fit are given in Table III and are in reasonable agreement with Kou et al.[3] but more precise. The root-mean-square deviations of the fits, 0.11×10^{-4} cm^{-1} for ν_5 hot bands and 0.82×10^{-4} cm^{-1} for ν_4 hot bands, are still several orders of magnitude larger than the

spectrometer accuracy. This suggests that there are some smaller perturbations that remain undetected using this simple analysis.

The results of these analyses are illustrated in Figure 5, where we plot the calculated energies, using the results in Table III subtracted from the "experimental" upper level energies, calculated as described above. There are multiple perturbations in the (10110) e/f levels, while the (10101) e/f levels show weaker perturbations in general, but a strong perturbation at J'_e=21. The patterns of the perturbations show that they derive from the crossing of perturbing levels associated with background vibrational levels at this excitation energy. This simple analysis is likely only identifying the larger perturbations since it depends to some extent on the precision of the older FTIR measurements. In the future, the Herman-Perry polyad Hamiltonian or a similar global model should be able to identify the active perturbing levels and the measurements in the current work will permit a refinement of the perturbation parameters involved.

4. Conclusions

A total of 135 transition frequencies for v_4=1 and v_5=1 hot band lines have been measured in the $\nu_1 + \nu_3$ band of C_2H_2 with absolute uncertainties of between 3 and 22 kHz. The comparison between measured line positions and those positions listed in the HITRAN2012 database reveals *J*-dependent differences of the order of 10's of MHz, not surprising since the HITRAN data derive from Doppler-limited FTIR measurements. By calculating the upper state level energies from known lower levels caused by near degeneracies of background combination vibrational excitations in the upper level of the observed transitions, it was possible to identify numerous small local perturbations in the upper levels. These will be useful in characterizing discrete interactions in the matrix representation of the interacting vibration-rotation levels in polyad or other global models of the vibration-rotation structure.

5. Acknowledgements

Work at Brookhaven National Laboratory is funded by the Division of Chemical Sciences, Geosciences and Biosciences within the Offices of Basic Energy Sciences, Office of Sciences, U.S. Department of Energy under Contract Nos. DE-AC02-98CH10886 and DE-SC00012704. We are most grateful to Prof. M. Herman (U.Bruxelles) and Prof. D.S Perry (U. of Akron) for providing us with detailed results from their work and helpful discussions. We also thank Dr D. Forthomme (BNL) for many helpful suggestions.

6. References

[1] M. Herman, *Molec. Phys.* 105 (2007) 2217-2241.

[2] K. Didriche, M. Herman, *Chem. Phys. Letts.* 496 (2010) 1-7.

[3] Q. Kou, G. Guelachvili, M.A. Temsamani, M. Herman, *Can. J. Phys.* 72 (1994) 1241-1250.

[4] K.A. Keppler, G.C. Mellau, S. Klee, B.P. Winnewisser, M. Winnewisser, J. Pliva, K.N. Rao, *J. Molec. Spectrosc.* 175 (1996) 411-420.

[5] R. El Hachtouki, J. Vander Auwera, *J. Molec. Spectrosc.* 216 (2002) 355-362.

[6] S. Robert, M. Herman, A. Fayt, A. Campargue, S. Kassi, A. Liu, L. Wang, G. Di Lonardo, L. Fusina, *Molec. Phys.* 106 (2008) 2581-2605.

[7] M. Herman, A. Campargue, M.I. El Idrissi, J. Vander Auwera, *J. Phys. Chem. Ref. Data.* 32 (2003) 921-1361.

[8] S. Robert, M. Herman, J. Vander Auwera, G. Di Lonardo, L. Fusina, G. Blanquet, M. Lepere, A. Fayt, *Molec. Phys.* 105 (2007) 559-568.

[9] B. Amyay, M. Herman, A. Fayt, A. Campargue, S. Kassi, *J. Molec. Spectrosc.* 267 (2011) 80-91.

[10] D.S. Perry, J. Martens, B. Amyay, M. Herman, *Molec. Phys.* 110 (2012) 2687-2705.

[11] O.M. Lyulin, J.V. Auwera, A. Campargue, *J. Quant. Spectrosc. Radiat. Transf.* 160 (2015) 85-93.

[12] O.M. Lyulin, V.I. Perevalov, J.-L. Teffo, in: L.N. Sinitsa, (Ed.), 14th Symposium on High Resolution Molecular Spectroscopy, SPIE, 2004.

[13] S. Yu, B.J. Drouin, J.C. Pearson, *Astrophys. J.* 705 (2009) 786.

[14] K. Nakagawa, M. De Labachelerie, Y. Awaji, M. Kourogi, *JOSA B* 13 (1996) 2708-2714.

[15] C.S. Edwards, H.S. Margolis, G.P. Barwood, S.N. Lea, P. Gill, G. Huang, W.R.C. Rowley, *Opt. Letts.* 29 (2004) 566-568.

[16] A.A. Madej, A.J. Alcock, A. Czajkowski, J.E. Bernard, S. Chepurov, *J. Opt. Soc. Amer. B* 23 (2006) 2200-2208.

[17] C.S. Edwards, G.P. Barwood, H.S. Margolis, P. Gill, W.R.C. Rowley, *J. Molec. Spectrosc.* 234 (2005) 143-148.

[18] N.J. Evans II, J.H. Lacy, J.S. Carr, *Astrophys. J.* 383 (2007) 674-692.

[19] S.T. Ridgway, *Astrophys. J.* 187 (1974) p. L41.

[20] A. Coustenis, *Space Science Reviews* 116 (2005) 171-184.

[21] R. Zander, C.P. Rinsland, D.H. Ehhalt, J. Rudolph, P. Demoulin, *J. Atmos. Chem.* 13 (1991) 359-372.

[22] J. Rudolph, D.H. Ehhalt, A. Khedim, *J. Atmos. Chem.* 2 (1984) 117-124.

[23] H.S. Margolis, *Chem. Soc. Rev.* 41 (2012) 5174-5184.

[24] M. Cich, C. McRaven, G. Lopez, T. Sears, D. Hurtmans, A. Mantz, *Applied Physics B: Lasers and Optics* (2011) 1-12.

[25] M.J. Cich, D. Forthomme, C.P. McRaven, G.V. Lopez, G.E. Hall, T.J. Sears, A.W. Mantz, *J. Phys. Chem. A* (2013).

[26] C.P. McRaven, M.J. Cich, G.V. Lopez, T.J. Sears, D. Hurtmans, A.W. Mantz, *J. Molec. Spectrosc.* 266 (2011) 43-51.

[27] M.J. Cich, D. Forthomme, G.E. Hall, C.P. Mcraven, T.J. Sears, S. Twagirayezu, The 13th Biennial HITRAN Conference (HITRAN13), Harvard-Smithsonian Center for Astrophysics, Cambridge, MA, USA.

[28] E.D. Black, *Am. J. Phys.* 69 (2001) 79-87.

[29] O. Axner, P. Kluczynski, Ö.M. Lindberg, *J. Quant. Spectrosc. Radiat. Transf.* 68 (2001) 299-317.

[30] A. Le Floch, R. Le Naour, J.M. Lenormand, J.P. Tache, *Phys. Rev. Letts.* 45 (1980) 544-547.

[31] W.T. Hill III, T.W. Hansch, A.L. Schawlow, *Appl. Opt.* 24 (1985) 3718-3724.

[32] W. Demtroeder, Laser Spectroscopy: Basic Conceptrs and Instrumentation, 2nd Ed. 2 ed.; Springer-Verlag, Berlin, 1996.

[33] M. Šimečková, D. Jacquemart, L.S. Rothman, R.R. Gamache, A. Goldman, *J. Quant. Spectrosc. Radiat. Transf.* 98 (2006) 130-155.

[34] B. Amyay, A. Fayt, M. Herman, *J. Chem. Phys.* 135 (2011) 234305(9).

[35] O.M. Lyulin, D. Jacquemart, N. Lacome, V. Perevalov, J.Y. Mandin, *J. Quant. Spectrosc. Radiat. Transf.* 109 (2008) 1856-1874.

[36] L.S. Rothman, I.E. Gordon, Y. Babikov, A. Barbe, D. Chris Benner, P.F. Bernath, M. Birk, L. Bizzocchi, V. Boudon, L.R. Brown, A. Campargue, K. Chance, E.A. Cohen, L.H. Coudert, V.M. Devi, B.J. Drouin, A. Fayt, J.M. Flaud, R.R. Gamache, J.J. Harrison, J.M. Hartmann, C. Hill, J.T. Hodges, D. Jacquemart, A. Jolly, J. Lamouroux, R.J. Le Roy, G. Li, D.A. Long, O.M. Lyulin, C.J. Mackie, S.T. Massie, S. Mikhailenko, H.S.P. Müller, O.V. Naumenko, A.V. Nikitin, J. Orphal, V. Perevalov, A. Perrin, E.R. Polovtseva, C. Richard, M.A.H. Smith, E. Starikova, K. Sung, S. Tashkun, J. Tennyson, G.C. Toon, V.G. Tyuterev, G. Wagner, *J. Quant. Spectrosc. Radiat. Transf.* 130 (2013) 4-50.

[37] D. Mazzotti, P. DeNatale, G. Guiusfredi, C. Fort, J.A. Mitchell, L. Hollberg, *Opt. Letts.* 25 (2000) 350-352.

7. Tables

Separate pdf files from the spreadsheets are attached.

8. Figure Captions

Figure 1. Experimental schematic for saturation dip spectroscopy. Extended Cavity Diode Laser (ECDL) is locked to absorption cell cavity through the Pound–Drever–Hall (PDH) technique[28]. The cavity is referenced to the frequency comb and the 830 Hz wavelength modulation is employed to enhance the sensitivity. The 830 Hz signal frequency is produced using a function generator (FG). This signal is then employed: (1) for modulating the output of voltage-controlled oscillator (VCO) set at 188MHz that drives electro-optic modulator (EOM), (2) as the reference frequency for adjustments of feed-forward and (3) as reference for the lock-in amplifier. PZT(1) and PZT(2) are Piezo-electric translators employed for tuning the cavity length. In order to tune through cavity modes, during the set up or troubleshooting, a DC offset is applied in long PZT(2). It is held fixed during data acquisition. Signal generator (SG) produces 192MHz frequency modulation for PDH lock. All frequencies are referenced to the GPS satellite time standard.

Figure 2. Saturation dip measurements (symbols) of P(11) in the $\nu_1 + \nu_3$ band of $^{12}C_2H_2$ at a pressure of 1 mTorr (0.13 Pa) as a function of intracavity laser power. Distortion from the best fit first derivative of a symmetrical Lorentzian profile (lines) and increased line width due to power broadening is clear at the higher powers.

Figure 3. Doppler-free transitions for v_4 =1 and v_5 =1 hot bands. The upper panel shows examples of typical saturation dip transmission signals. The circle symbols represent observed experimental data points and the lines are result fit of the data in order to determine the line center (see text for more details) with the fitted line center in GHz and the estimated error in units of the last quoted significant figure. The lower panel is an overview stick representation of all lines measured in this work with intensities from the HITRAN 2012 database[36] for illustrative purposes.

Figure 4. Differences between the measured frequencies for transitions in the v_4 =1 and v_5 =1 hot bands in the $\nu_1 + \nu_3$ band and those quoted in the HITRAN 2012 database. Note, Q-branch lines are not shown as they are not included in the HITRAN database. The transitions are labeled by *m*: *m* = -*J* for *P*-branch transitions and *m* = *(J+1)* for *R*-branch transitions. Perturbations in the higher *J P*-branch lines for the v_4 hot band are clear.

Figure 5. Plots of observed upper level term values minus the term values calculated from a polynomial fit of the form given in Eq. 4 to unperturbed levels, illustrating the *J*-dependent perturbations in the (1011^10^0) and (1010^01^1) levels. The superscripts on the v_4 and v_5 quantum numbers are l_4 and l_5, respectively.

Table I. Measured line positions for ν_4 =1 hot band lines in the ν_1+ ν_3 region of C_2H_2

J''	Frequency/ GHz	Wavenumber/ cm^{-1}	Unc. / kHz[a]	Diff. /MHz[b]	Sample Pressure / mTorr
$P_e(30)$	193320.0108658	6448.461450814	16.1	-106	20
$P_e(29)$	193412.1033288	6451.533324726	5.2	61	20
$P_e(28)$	193503.2722645	6454.574393079	11.3	42	20
$P_e(27)$	193593.7389656	6457.592037408	4.0	1	21
$P_e(26)$	193683.4864356	6460.585690770	7.2	6	21
$P_e(25)$	193772.5102190	6463.555204548	5.5	-6	20
$P_e(24)$	193860.8089037	6466.500531635	8.9	-17	21
$P_e(23)$	193948.3755854	6469.421441728	3.3	-32	20
$P_e(22)$	194035.1994196	6472.317573100	4.7	-61	19
$P_e(21)$	194121.2668482	6475.188473496	3.5	-115	20
$P_e(20)$	194206.9890395	6478.047858012	4.1	218	20
$P_e(19)$	194291.4605977	6480.865525900	3.6	34	20
$P_e(18)$	194375.3619464	6483.664173645	5.6	14	23
$P_e(16)$	194540.9743445	6489.188408618	5.1	-6	22
$P_e(14)$	194703.6430557	6494.614452764	7.9	-13	25
$P_e(12)$	194863.3495525	6499.941685324	3.4	-15	10
$P_e(7)$	195249.5770192	6512.824849624	4.0	-11	5
$P_e(6)$	195324.5762894	6515.326555994	5.1	-7	18
$P_e(5)$	195398.8238428	6517.803187791	4.7	-6	15
$P_e(4)$	195472.3184659	6520.254704536	4.3	-6	25
$Q_e(1)$	195758.3103901	6529.794368279	3.7	-	20
$Q_e(2)$	195757.4462571	6529.765543905	12.1	-	20
$P_e(3)$	195545.0588664	6522.681063123	4.2	-4	15
$P_e(2)$	195617.0438081	6525.082222320	8.0	-5	26
$R_e(1)$	195897.4050151	6534.434065554	4.7	-4	30
$R_e(2)$	195965.5948524	6536.708633692	8.3	-5	17
$R_e(3)$	196033.0221908	6538.957767604	4.4	-7	13
$R_e(4)$	196099.6859557	6541.181431445	4.2	-8	17
$R_e(5)$	196165.5850261	6543.379583285	3.2	-9	12
$R_e(6)$	196230.7185636	6545.552206320	3.6	-8	16

Table I. Measured line positions for ν_4 =1 hot band lines in the ν_1+ ν_3 region of C_2H_2

J''	Frequency/ GHz	Wavenumber/ cm^{-1}	Unc. / kHz[a]	Diff. /MHz[b]	Sample Pressure / mTorr
$R_e(7)$	196295.0833720	6547.699187682	3.5	-12	17
$R_e(8)$	196358.6826815	6549.820632294	3.5	-14	12
$R_e(9)$	196421.5123556	6551.916404633	3.3	-15	15
$R_e(11)$	196544.8609562	6556.030871069	3.3	-13	18
$R_e(12)$	196605.3780535	6558.049494876	3.5	-12	20
$R_e(13)$	196665.1226863	6560.042370589	3.5	-10	7
$R_e(14)$	196724.0943691	6562.009454189	3.6	-4	20
$R_e(15)$	196782.2927096	6563.950741871	4.3	1	10
$P_f(30)$	193316.4650753	6448.343175975	8.9	5	20
$P_f(29)$	193408.3175387	6451.407044359	15.7	-2	20
$P_f(28)$	193499.4614339	6454.447277453	6.0	-22	20
$P_f(27)$	193589.8743277	6457.463126964	10.0	-26	21
$P_f(26)$	193679.6179908	6460.456653342	4.2	-25	21
$P_f(25)$	193768.6134340	6463.425221790	10.7	-47	20
$P_f(24)$	193856.8005977	6466.366828937	4.2	-167	20
$P_f(23)$	193944.6741872	6469.297976374	7.2	113	18
$P_f(22)$	194031.4714773	6472.193222330	3.7	34	19
$P_f(21)$	194117.6099888	6475.066493794	9.4	15	30
$P_f(20)$	194203.0382578	6477.916074119	4.0	5	20
$P_f(18)$	194371.7411707	6483.543397568	3.3	5	17
$P_f(16)$	194537.5559948	6489.074384745	3.6	-9	15
$P_f(14)$	194700.4693778	6494.508590267	5.5	-12	25
$P_f(12)$	194860.4703688	6499.845648847	3.1	-14	10
$P_f(7)$	195247.6635296	6512.761022480	4.8	-8	8
$P_f(6)$	195322.8958755	6515.270503418	4.1	-6	10
$P_f(5)$	195397.3899095	6517.755356925	5.5	-7	20
$P_f(4)$	195471.1444173	6520.215542492	5.0	-5	14
$P_f(3)$	195544.1581514	6522.651018506	8.4	-5	18
$Q_f(4)$	195748.0164940	6529.451000865	8.8	-	20
$Q_f(1)$	195757.6697964	6529.773000375	9.1	-	20
$P_f(2)$	195616.4299346	6525.061745703	4.9	-5	25

Table I. Measured line positions for ν_4 =1 hot band lines in the ν_1+ ν_3 region of C_2H_2

J''	Frequency/ GHz	Wavenumber/ cm^{-1}	Unc. / kHz[a]	Diff. /MHz[b]	Sample Pressure / mTorr
$R_f(1)$	195898.0722980	6534.456323713	6.1	-5	32
$R_f(2)$	195966.6157757	6536.742688026	4.9	-6	17
$R_f(3)$	196034.4100199	6539.004060600	4.7	-7	24
$R_f(4)$	196101.4538416	6541.240401772	3.4	-6	15
$R_f(5)$	196167.7460930	6543.451673257	5.8	-7	14
$R_f(6)$	196233.2856102	6545.637836234	3.2	-8	12
$R_f(7)$	196298.0711991	6547.798850866	3.9	-11	16
$R_f(8)$	196362.1024211	6549.934702530	3.4	-9	15
$R_f(9)$	196425.3744949	6552.045231735	3.9	-12	10
$R_f(10)$	196487.8919135	6554.130588350	3.1	-12	13
$R_f(11)$	196549.6502875	6556.190625967	3.5	-12	20
$R_f(12)$	196610.6489680	6558.225322934	3.1	-11	12
$R_f(13)$	196670.8869955	6560.234647249	6.3	-11	17
$R_f(14)$	196730.3631463	6562.218558091	3.2	-10	20
$R_f(15)$	196789.0766510	6564.177029796	4.0	-8	20

[a]Estimated errors given by $\sqrt{(\delta^2 + \text{Unc.}^2)}$, where δ represents the accuracy of the spectrometer (3kHz) while Unc. is RMSE resulting from the fit of measured line postion to lineshape function.

[b]Obtained by subtracting the line position data in HITRAN 2012 from measured line position.

Table II. Measured line positions for ν_5=1 hot band lines in the $\nu_1+\nu_3$ region of $^{12}C_2H_2$

J''	Frequency/ GHz	Wavenumber/ cm^{-1}	Unc. /kHz[a]	Diff. / MHz[b]	Sample Pressure / mTorr
$P_e(28)$	193643.2421315	6459.243285283	6.1	-3.4	20
$P_e(27)$	193734.2416788	6462.278703450	9.4	0.1	25
$P_e(26)$	193824.4943752	6465.289209349	4.7	-2.7	20
$P_e(25)$	193914.0084276	6468.275076740	8.1	-3.7	22
$P_e(24)$	194002.7781161	6471.236114822	3.7	-2.6	19
$P_e(22)$	194178.0871192	6477.083793723	6.4	-3.2	17
$P_e(20)$	194350.4066032	6482.831752998	4.6	-1.4	20
$P_e(19)$	194435.4368543	6485.668056875	8.3	-4.3	20
$P_e(18)$	194519.7243607	6488.479585457	4.8	-0.4	20
$P_e(16)$	194686.0313389	6494.026989126	3.5	-3.3	23
$P_e(14)$	194849.3171214	6499.473616558	4.4	-2.9	10
$P_e(13)$	194929.8236349	6502.159024789	3.8	-2.4	22
$P_e(12)$	195009.5709002	6504.819107231	7.2	-2.8	15
$P_e(10)$	195166.7822407	6510.063113084	4.2	-5.6	20
$P_e(9)$	195244.2438235	6512.646953362	13.6	-4.4	16
$P_e(8)$	195320.9409311	6515.205293492	4.9	-6.2	25
$P_e(7)$	195396.8725988	6517.738101297	6.4	-6.0	28
$P_e(6)$	195472.0370523	6520.245317588	6.1	-5.5	26
$P_e(4)$	195620.0604283	6525.182845938	21.8	-7.6	20
$P_e(3)$	195692.9169314	6527.613077292	7.5	-7.1	30
$P_e(2)$	195765.0015526	6530.017561437	6.5	-7.4	20
$Q_e(1)$	195906.3688749	6534.733067731	10.3	-	20
$R_e(3)$	196181.2354031	6543.901628210	4.4	-5.6	14
$R_e(4)$	196247.8845690	6546.124805081	3.5	-5.4	12
$R_e(5)$	196313.7525768	6548.321925322	7.4	-5.2	7
$R_e(6)$	196378.8385643	6550.492960177	3.2	-4.2	12
$R_e(7)$	196443.1411973	6552.637865135	4.5	-3.8	25
$R_e(8)$	196506.6594132	6554.756604758	3.3	-5.6	24
$R_e(10)$	196631.3384055	6558.915448282	3.9	-4.5	10
$R_e(12)$	196752.8670494	6562.969207499	3.3	-2.8	15
$P_f(27)$	193730.7499470	6462.162231812	4.6	1.0	20
$P_f(26)$	193820.9869807	6465.172215262	7.1	-2.5	23
$P_f(25)$	193910.4935381	6468.157832646	4.2	-2.0	20
$P_f(24)$	193999.2668270	6471.118990825	6.4	-3.3	19

Table II. Measured line positions for ν_5=1 hot band lines in the $\nu_1+\nu_3$ region of $^{12}C_2H_2$

J''	Frequency/ GHz	Wavenumber/ cm^{-1}	Unc. /kHz[a]	Diff. / MHz[b]	Sample Pressure / mTorr
$P_f(22)$	194174.6089573	6476.967774729	13.2	-6.8	20
$P_f(20)$	194347.0183310	6482.718732405	10.3	1.0	20
$P_f(19)$	194432.1120446	6485.557153162	5.3	-1.4	20
$P_f(18)$	194516.4657450	6488.370889736	7.2	-1.4	20
$P_f(16)$	194682.9480470	6493.924141580	5.1	-0.3	25
$P_f(14)$	194846.4546031	6499.378133226	3.3	-2.4	14
$P_f(13)$	194927.0888981	6502.067803792	3.5	-0.1	23
$P_f(12)$	195006.9755551	6504.732535835	12.7	-1.9	20
$P_f(10)$	195164.5009025	6509.987015835	9.6	-2.5	20
$P_f(9)$	195242.1371243	6512.576681443	5.8	-3.6	14
$P_f(8)$	195319.0207563	6515.141243356	11.0	-4.7	18
$P_f(7)$	195395.1507555	6517.680666788	5.7	-4.0	20
$P_f(6)$	195470.5254034	6520.194894410	6.6	-6.2	15
$P_f(3)$	195692.1075619	6527.586079630	5.6	-6.4	25
$P_f(2)$	195764.4500171	6529.999164192	10.4	-7.0	30
$Q_f(1)$	195905.7935779	6534.713877888	5.7	-	16
$R_f(3)$	196182.4804847	6543.943159660	3.5	-7.5	14
$R_f(4)$	196249.4702451	6546.177697542	6.7	-5.8	13
$R_f(5)$	196315.6904643	6548.386566293	4.5	-4.0	25
$R_f(6)$	196381.1400952	6550.569730983	5.0	-5.1	15
$R_f(7)$	196445.8179246	6552.727151150	3.5	-4.1	25
$R_f(8)$	196509.7226386	6554.858782958	3.5	-3.4	24
$R_f(9)$	196572.8531830	6556.964591251	6.9	-3.3	22
$R_f(10)$	196635.2083179	6559.044534666	5.3	-2.0	10
$R_f(12)$	196757.5878691	6563.126677093	5.2	-0.7	15.0

[a]Estimated errors given by $\sqrt{(\delta^2+\text{Unc.}^2)}$, where δ represents the accuracy of the spectrometer (3 kHz) while Unc. is RMSE resulting from the fit of measured line postion to lineshape function.

[b]Obtained by subtracting the line position data in HITRAN 2012 from measured line position

Table III: Rotational parameters derived from fitting unperturbed levels

	Parameter	Upper Level /cm^{-1} This Work[a]	Upper Level /cm^{-1} FTS[b]	Lower Level /cm^{-1} FTS[c]
	ν_0	6534.7363088 (34)	6534.736540 (55)	
	B	1.165954510 (61)	1.16595300 (49)	1.178787168
	D (x10^6)	1.64285 (24)	1.6394 (10)	1.651628
ν_5	H (x10^{12})	2.29 (25)		1.6
	q_B (x10^3)	4.895855 (41)	4.89531 (28)	4.69842
	q_D (x10^8)	-4.730 (8)	-4.651 (37)	-3.8477
	RMS (x10^3)	0.011	0.2	
	ν_0	6529.796178 (20)	6529.79636 (12)	
	B	1.16538975 (39)	1.1653915 (13)	1.17793497
	D (x10^6)	1.6572 (18)	1.6613 (31)	1.659681
ν_4	H (x10^{12})	10 (2)	11.7 19	1.6
	q_B (x10^3)	5.45334 (29)	5.45271 (71)	5.23075
	q_D (x10^8)	-4.86 (5)	-4.67 (10)	-3.9301
	RMS (x10^3)	0.082	0.5	

[a] Upper state constants obtained from present data by fitting the upper state term values to a $J(J+1)$ polynomial expansion (eq.4). The numbers in parentheses are standard deviation in units of the last digits.

[b] Upper state FTS constants obtained from reference [3]. The numbers in parentheses are standard deviation in units of the last digits.

[c] Quoted in reference [3], from work by Y. Kabbadj, M.Herman, G.DiLonardo, L. Fusina and J.W.C. Johns, J. Molec. Spectrosc. 150, 535 (1991).

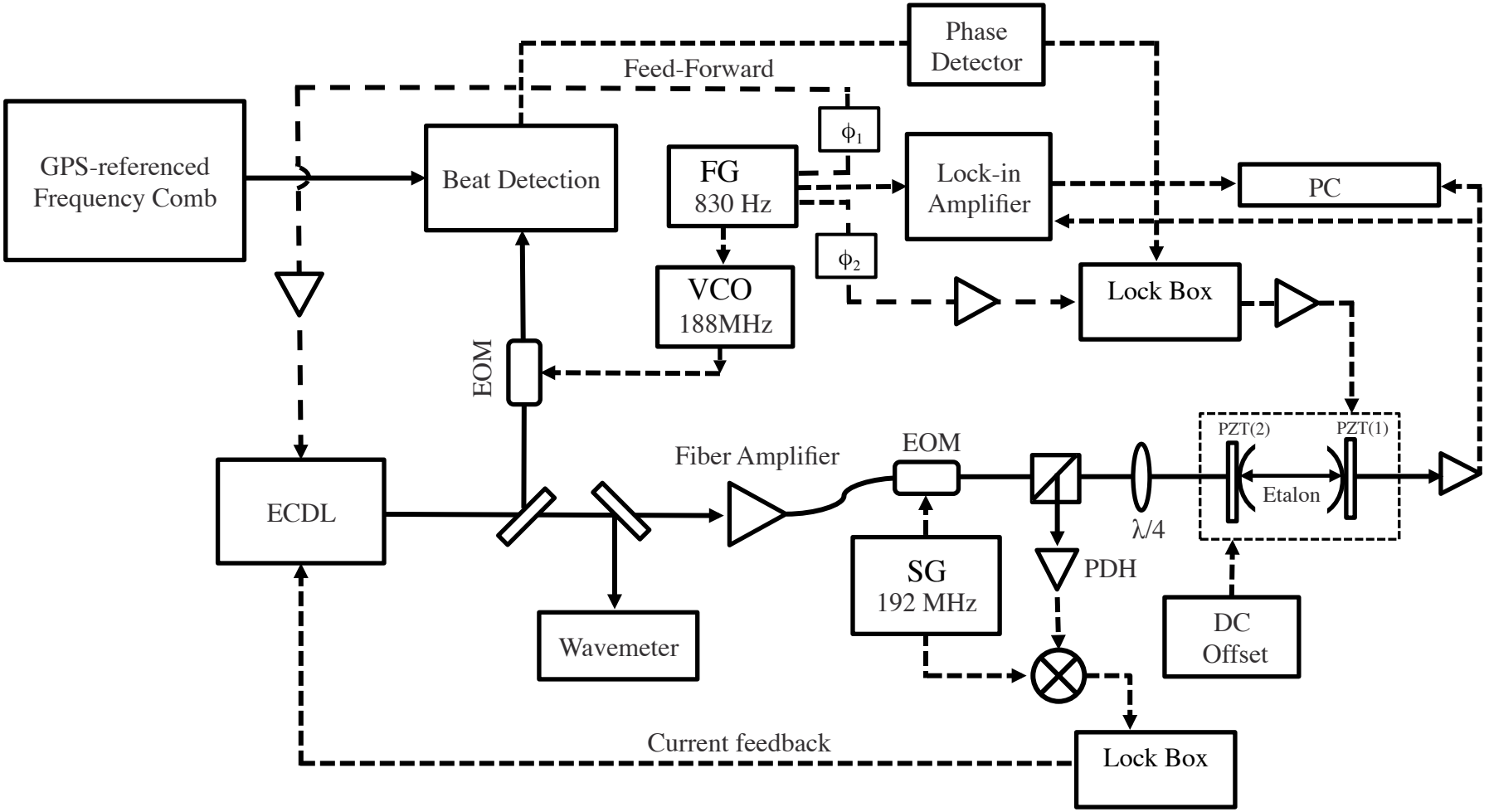
Phase Detector
Feed-Forward
GPS-referenced Frequency Comb
Beat Detection
FG 830 Hz
ϕ_1
ϕ_2
Lock-in Amplifier
PC
VCO 188MHz
Lock Box
EOM
PZT(2)
PZT(1)
Fiber Amplifier
EOM
ECDL
Etalon
$\lambda/4$
SG 192 MHz
PDH
DC Offset
Wavemeter
Current feedback
Lock Box

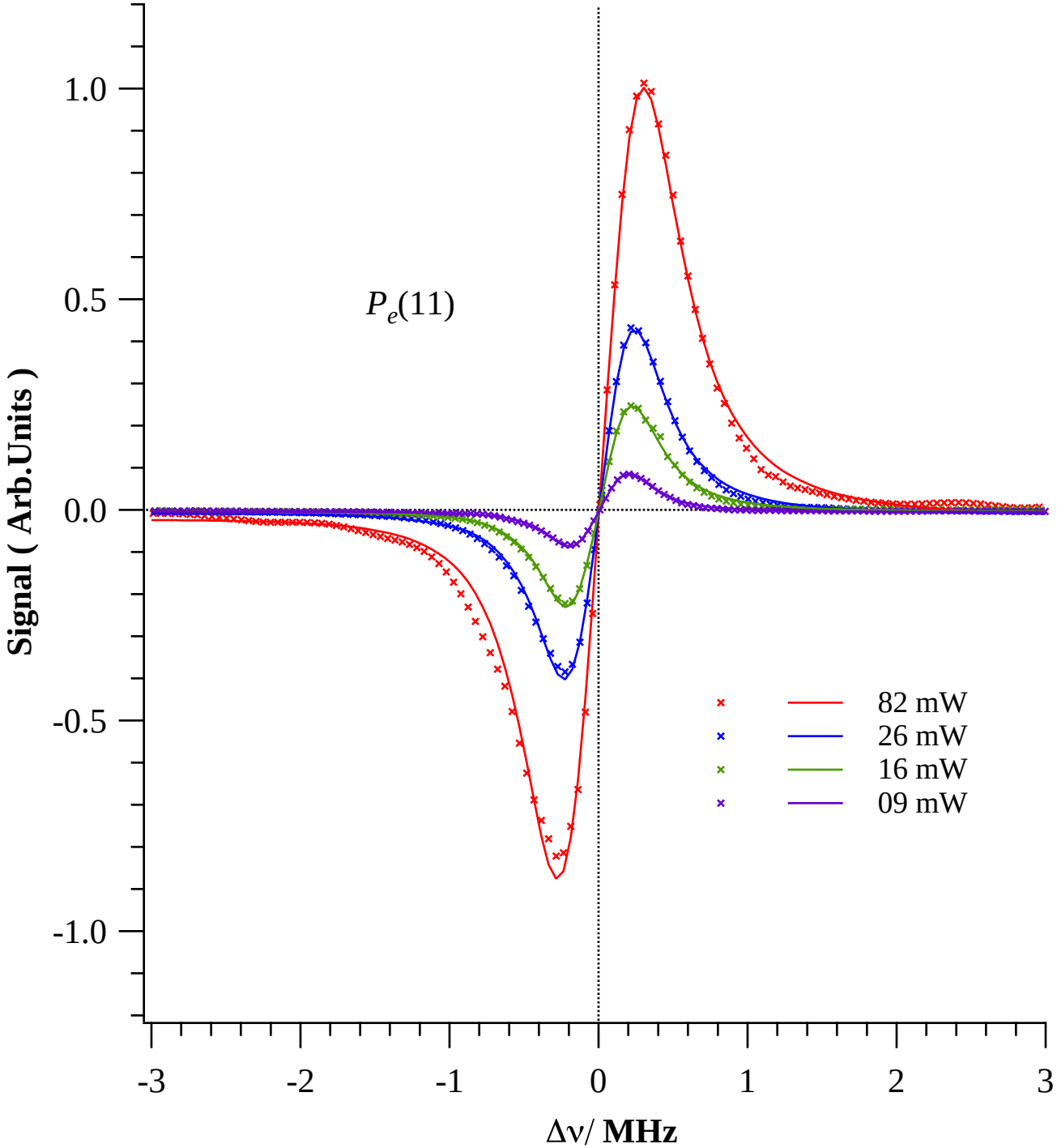
1.0
0.5
0.0
-0.5
-1.0
Signal (Arb.Units)
$P_e(11)$
82 mW
26 mW
16 mW
09 mW
-3
-2
-1
0
1
2
3
Δν/ MHz

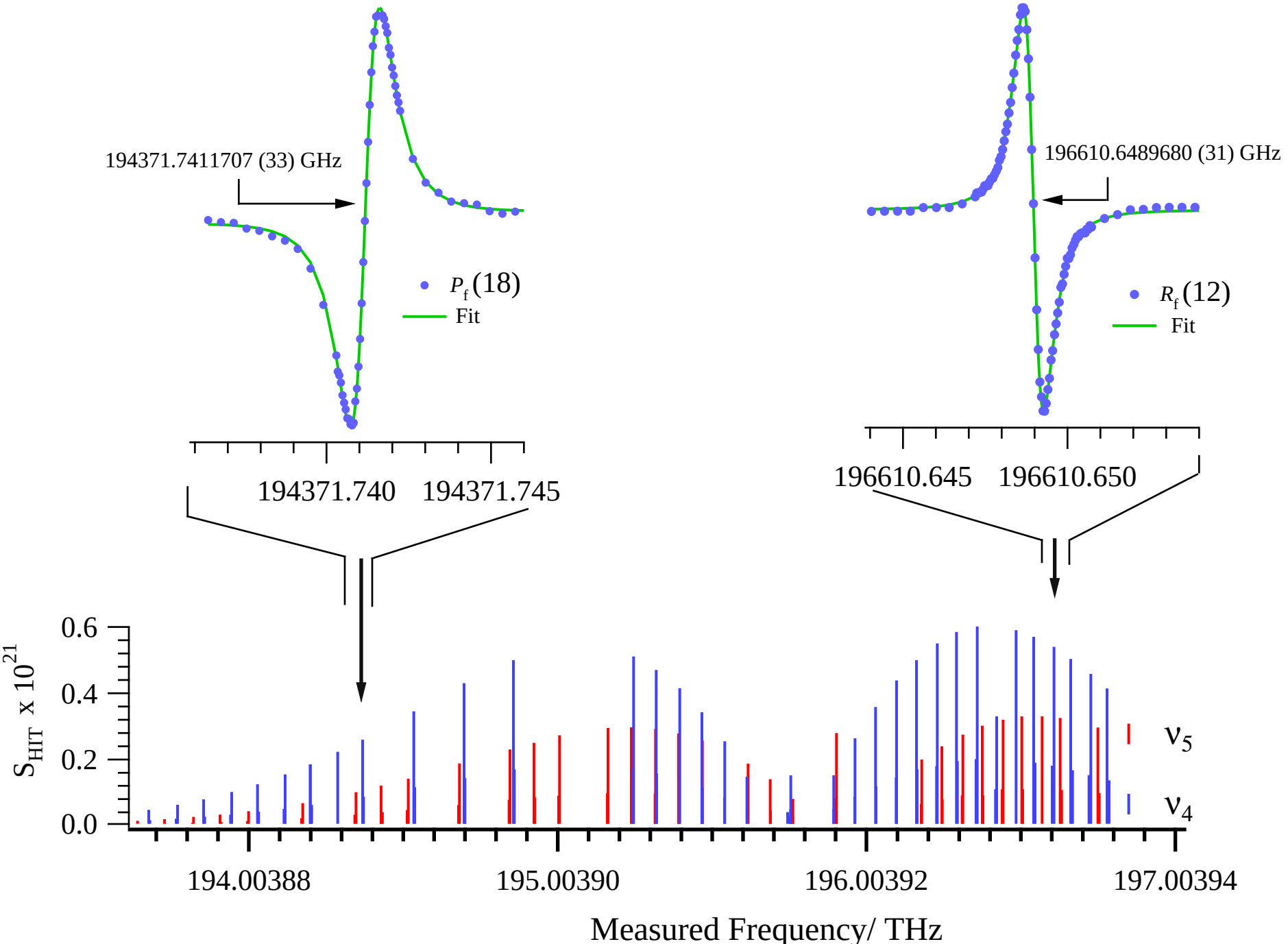
194371.7411707 (33) GHz
$P_f(18)$
Fit
194371.740
194371.745
196610.6489680 (31) GHz
$R_f(12)$
Fit
196610.645
196610.650
S_{HIT} x 10^{21}
0.6
0.4
0.2
0.0
ν_5
ν_4
194.00388
195.00390
196.00392
197.00394
Measured Frequency/ THz

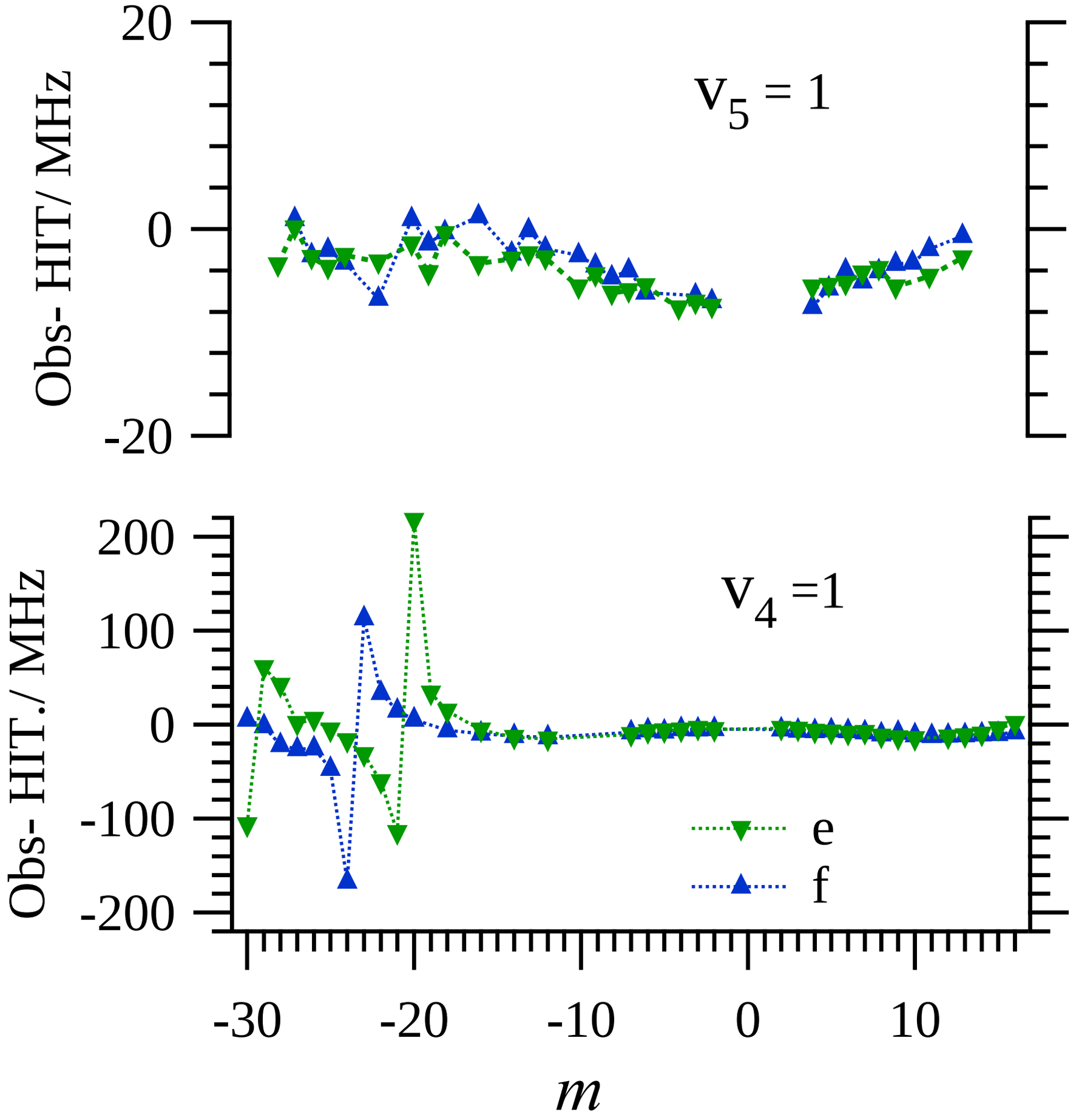
20
0
-20
Obs- HIT/ MHz
v5 = 1
200
100
0
-100
-200
Obs- HIT./ MHz
v4 =1
e
f
-30
-20
-10
0
10
m

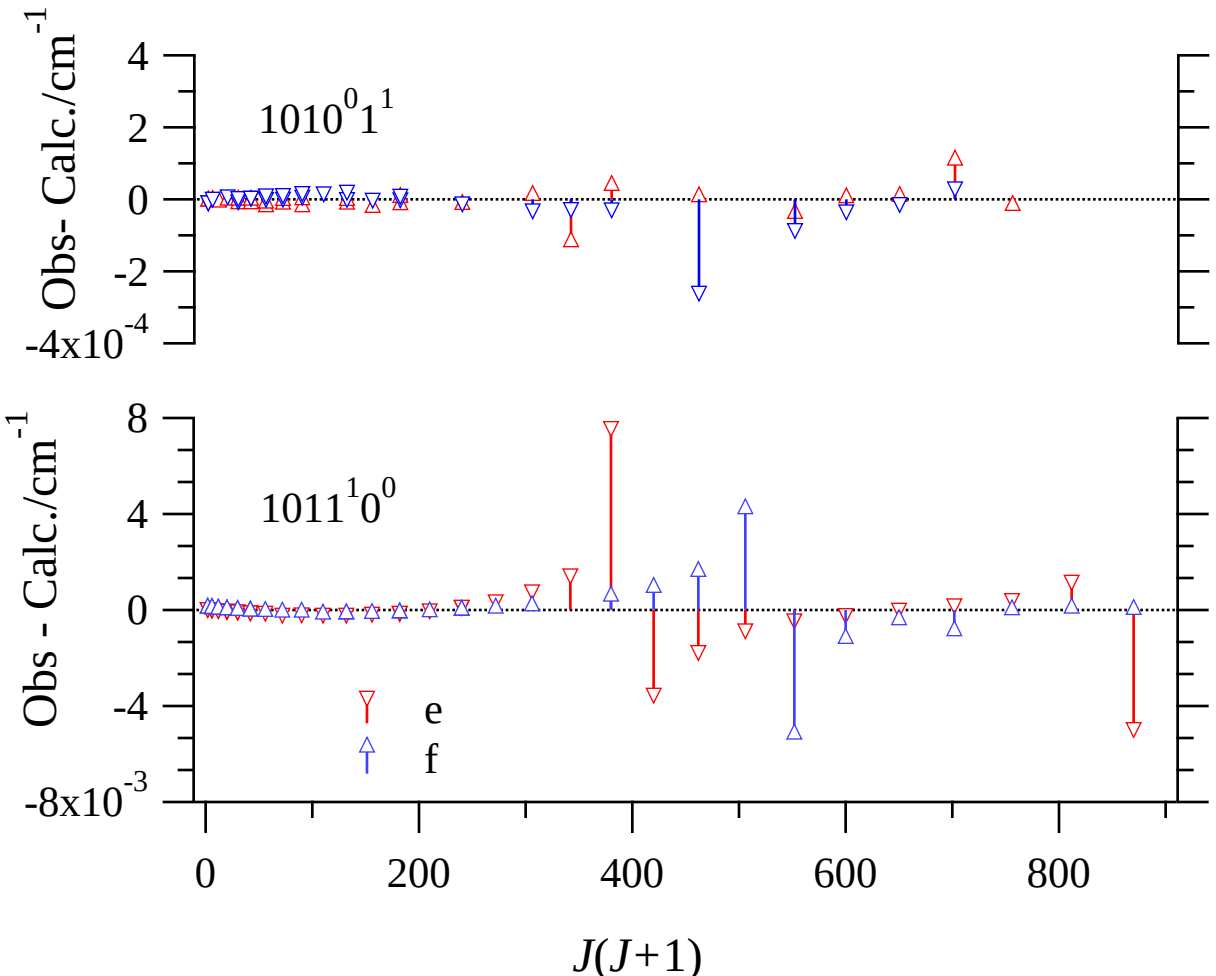
Obs- Calc./cm-1
4
2
0
-2
-4x10-4
1010^0 1^1
Obs - Calc./cm-1
8
4
0
-4
-8x10-3
1011^1 0^0
e
f
0
200
400
600
800
J(J+1)